PEER REVIEWED

ABSTRACT

Previous papers have described the effect of blade width, blade shape, wire tension, and wire wrap angle on the pressure pulses generated by a single blade in twin-wire blade forming. This paper considers the influence of applied suction in the suction shoe on the same pressure pulse generation.

As a result of applied suction, the forming fabric exposed to the suction is pulled down between the forming blades, producing arced shapes rather than the nearly linear fabric profiles that characterize a forming shoe without suction. The suction also causes substantially more dewatering to occur from the suction side (bottom wire) than from the other side (top wire) of the web. This difference in dewatering causes more fibers to adhere to the bottom wire side than to the top wire side, leading to significant two-sidedness of the paper sheet. All of these phenomena are modeled in a new computer code that has been developed to simulate suction shoe dewatering. The computer simulation developed here can also be used to calculate dewatering over the multiple blades that comprise a forming shoe without applied suction.

Discussion of the results of the computer simulation and comparison with mill trials will be left to a companion paper.

Application:

A theoretical analysis of suction shoe behavior, which has some experimental backing, is presented. This analysis is part of an extended model that describes formation and retention in the forming section of a paper machine.

Modeling suction shoes in twin-wire blade forming: theory

SHELDON I. GREEN

IN THE PAST 4 YEARS, THERE HAS BEEN a flurry of activity in modeling twin-wire blade formers. Zhao and Kerekes *(1)* developed the first, one-dimensional, analytical model of blade forming. They modeled a single, infinitesimal-width blade wrapped by two fabrics making prescribed angles to the blade, far upstream and downstream of the blade. A key result of their research was that such a forming geometry produces a single pressure pulse, which is located immediately upstream of the blade—a finding that was confirmed in pilot paper machine trials. Green, Zhao, and Kerekes followed up that research by developing a one-dimensional computer simulation that computes the behavior of flat, finite-width blades and shaped finite-width blades *(2–5)*. Those authors have shown that wide, flat blades generate two pressure pulses, one associated with wire wrap at the blade heel and one with wire wrap at the toe of the blade. Those pulses merge into a single pulse as the blade width narrows. Shaped wide blades produce two distinct pressure pulses when the blade shape is nearly flat, but only a single broad pulse is generated by a more parabolic blade shape. Green, Roshanzamir, and Kerekes have recently presented an extension of that work that includes a complete two-dimensional, viscous flow computation of the pressure pulse developed in a blade former *(6)*. That study confirms the principal results of the previous work. The three forming configurations that have been modeled previously are shown in **Fig. 1.**

In parallel work, Zahrai, Bark, and Norman *(7–9)* have developed a two-dimensional, inviscid flow model of twin-wire blade forming. Their work, completed before the two-dimensional, viscous model of Roshanzamir, Green, and Kerekes, is in excellent agreement with that model. Their work shows that, upstream of the blade in a twin-wire former, there is little z-direction variation in the fluid pressure. Downstream of the blade, however, there is a significant suction generated near the fabric in contact with the blade, which is a consequence of acceleration of fluid around the sharp corner generated by the blade heel.

The three forming configurations described thus far represent increasing levels of faithfulness in modeling the actual geometry of a paper machine. One feature of real paper machines that has been absent from these models is a suction shoe. That absence is addressed in this paper. In the course of solving for the behavior of a suction shoe, the multiple forming blades that exist in a forming shoe without suction are also modeled.

MODELING THE SUCTION SHOE

When suction is applied to a forming geometry, such as that shown in **Fig. 2,** the forming fabrics are drawn down between the blades. In consequence, the blade wrap angles α_1 and α_2 are not defined. Rather, the amount of wrap locally around a blade is a function of the applied

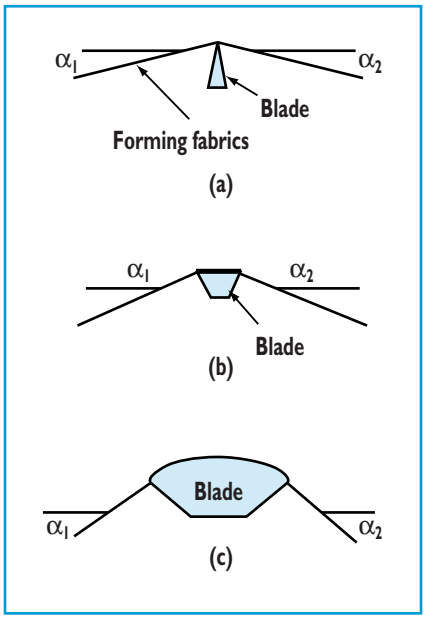

1. Different forming geometries studied previously. (a) Infinitesimal blade with prescribed wrap angle, (b) finite-width, flat blade with prescribed wrap angles, (c) shaped blade with prescribed wrap angles.

suction and the shoe geometry. In blade forming without suction, almost identical amounts of dewatering occur from the two fabrics, except over a blade itself. With applied suction, in contrast, significantly more water would be expected to be drawn off on the side of the suction shoe. This asymmetrical dewatering would result in more fiber deposition on the suction-side wire than on the other wire. With more fibers deposited on the suction-side wire, there is a concurrent increase in the drainage resistance of the suction-side fiber mat. Both the wire wrap effect and the variable mat drainage resistance are modeled here.

Variable drainage resistance model

Consider a wire with adhering fiber mat aligned with the x direction. The wire moves with velocity V_o. Let the drainage resistance of the wire and fiber mat, $R(x)$, be just the sum of the drainage resistance of the wire (R_{wire}) and the mat (R_{mat}) separately:

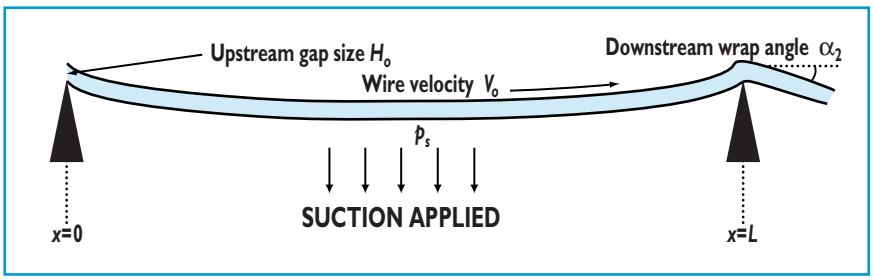

2. Forming geometry with applied suction in the suction shoe

$$R(x) = R_{wire} + R_{mat}(x) \qquad (1)$$

Provided that the fiber mat behaves as a thick, porous, incompressible medium, the drainage resistance of the fiber mat is directly proportional to the number of fibers on the wire per unit area, which I denote by $N(x)$. In Eq. 2, C_1 is a constant:

$$R_{mat} = C_1 N(x) \qquad (2)$$

Imagine that the pulp fibers are uniformly dispersed in the suspension, in the direction normal to the wire, with local concentration $C(x)$. These fibers accumulate on the wire in a filtration type of process. The number of fibers adhering to the wire in a time Δt, per unit wire area, is calculated as the velocity normal to the wire, $W(x)$, multiplied by both the local fiber concentration and the time increment[1]:

$$N(x) = W(x)\, C(x)\, \Delta t \qquad (3)$$

In the time Δt, the wire moves from location x to location $x+\Delta x$, where $\Delta x = \Delta t V_o$. Thus, in the time Δt, the mat resistance increases by $C_1 W(x)\, C(x)\, \Delta t$. Using Eq. 1, this is:

$$R(x + \Delta x) - R(x) = C_1\, W(x)\, C(x)\, \Delta t \qquad (4)$$

Dividing Eq. 4 by Δx and allowing Δx to approach zero results in the following differential equation governing the drainage resistance of this forming wire and fiber mat:

$$dR/dx = C_1\, W(x)\, C(x) / V_o \qquad (5)$$

If the fibers stay in contact with the wire (or the fiber mat adhering to the wire), once they touch it, then $C(x)$ is just a constant that is equal to the fiber concentration in the headbox. On the other hand, if "backwash" causes fibers to separate from the wire (i.e., it is possible to resuspend fibers), then $C(x)$ can increase with x. I assume here that $C(x)$, the fiber concentration between the wires, is constant. Then, Eq. 5 is simply:

$$dR/dx = C_2\, W(x) / V_o \qquad (6)$$

where C_2 is a constant that is dependent on the headbox consistency, the fiber furnish, and the ability of the forming fabric to retain fines.

If the wire and mat behave as a Darcy's Law medium (i.e., if the drainage velocity is sufficiently slow), then the velocity $W(x)$ through the wires is proportional to the local pressure $p(x)$ and inversely proportional to the local drainage resistance:

$$W(x) = p(x) / R(x) \qquad (7)$$

The top and bottom wires do not necessarily have the same drainage resistance. Eqs. 6 and 7 can therefore be combined to yield separate equations governing the drainage resistance of the two wires:

$$dR_1/dx = C_2 p_1(x) / [R_1(x) V_o] \qquad (8)$$

$$dR_2/dx = C_2 p_2(x) / [R_2(x) V_o] \qquad (9)$$

[1] This model is a reasonable one for the drainage characteristics of a pure fiber mat. The retention of fines is a strong function of both basis weight and dewatering velocity *(10)*, and therefore the model is less accurate with fines present.

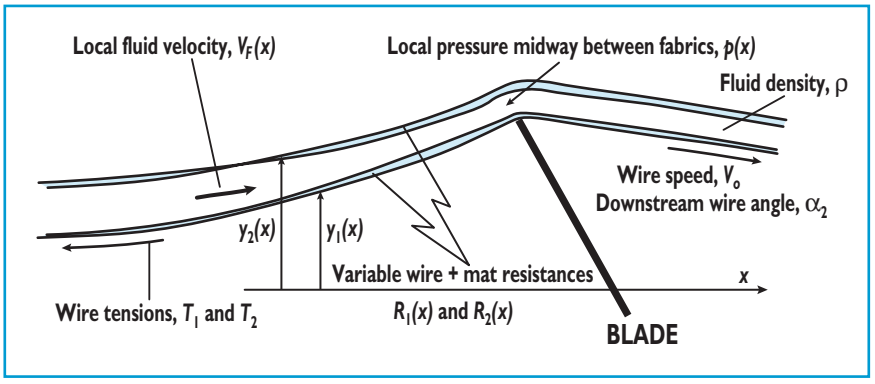

3. Detailed view of a blade gap former, showing many salient physical variables

The variable $p_1(x)$ is the pressure on the stock side of the fiber mat adhering to wire 1 (wire 1 is the bottom wire); the variable $p_2(x)$ is defined similarly. Owing to centrifugal forces in the fluid, these two pressures will be different. For the geometry shown in Fig. 2, the pressure at wire 1 will be somewhat higher than the pressure at wire 2 (the top wire) due to the streamline curvature. If the pressure midway between the wires is denoted by $p(x)$, the midline between the wires has a local radius of curvature *(RC),* the local stock velocity is V_F, and the perpendicular distance between the wires is H, then the pressure at wire 1 is given by:

$$p_1(x) = p(x) + (\rho V_F^2 H) / [2(RC)] \quad (10)$$

Similarly for wire 2:

$$p_2(x) = p(x) - (\rho V_F^2 H) / [2(RC)] \quad (11)$$

When the results are examined, a typical wire radius of curvature is found to be about 2 m. A normal gap size is 3 mm, and the fluid velocity is very nearly the wire velocity (about 16 m/s). Therefore, the pressure difference from wire 1 to wire 2 due to centrifugal effects is about 500 Pa. Given that a typical peak pressure pulse developed in a gap former is only about 8000 Pa (the average pulse is just 1000–2000 Pa), this centrifugal effect is clearly not insignificant.

Denoting the wire 1 position and slope by $y_1(x)$ and $dy_1(x)/dx$, respectively—and similarly for wire 2—then the value of $H/(RC)$ (the separation distance of the two fabrics divided by their mean radius of curvature) appearing in Eqs. 10 and 11 becomes to first-order:

SEE "OVERSIZED EQUATIONS" FOR EQUATION 12, p. 142.

In Eq. 12, $\overline{d^2y/dx^2}$ is the mean value of the second derivatives of the wire 1 and wire 2 shapes. Equations 8–12 must be solved simultaneously with equations governing the wire shapes and the flow between the forming wires.

Wire deflection model

In a previous paper, the modeling of finite-width forming blades has been discussed *(3).* The ideas presented there carry over to the physics of blades with suction. Consequently, to focus on just the effects arising from suction shoe suction, I will model forming fabrics sucked down between two infinitesimal blades. The finite-blade-width research can be coupled with the analysis performed here. None of the main conclusions of that work [(a) multiple blade pulses over wide blades and (b) pressure pulse shape changes with modest variations in blade shape] are altered by the research presented here.

The simulated geometry is shown in **Fig. 3.** This figure shows a detailed view of a portion of the forming geometry, with many additional variables labeled.

In addition to the equations discussed previously, four equations govern the behavior of a blade former. Those four equations are (a) an equilibrium equation for the bottom wire (the fabric in contact with the blades), (b) an equilibrium equation for the top wire (the fabric that is not in contact with the blades), (c) the continuity equation for the fluid filling the gap, and (d) the momentum equation for the same fluid:

SEE "OVERSIZED EQUATIONS" FOR EQUATIONS 13–16, p. 142.

Equations 8–11 and 13–16 determine, in addition to R_1 and R_2, the following six unknowns:

- The vertical displacement of the top wire (y_2) as a function of distance along the wire (x)
- The vertical displacement of the bottom wire (y_1) as a function of distance along the wire
- The pressure in the fluid immediately adjacent to the bottom wire (p_1) as a function of distance along the wire
- The pressure in the fluid immediately adjacent to the top wire (p_2) as a function of distance along the wire
- The pressure in the fluid midway between the fabrics (p) as a function of distance
- The average fluid velocity between the wires (V_F) as a function of distance.

The constants and fixed variables in the above equations are:

- The bending stiffness of the bottom wire [$(EI)_1$]. The bottom wire comes into physical contact with the blades.
- The tension per unit length in the bottom wire (T_1)

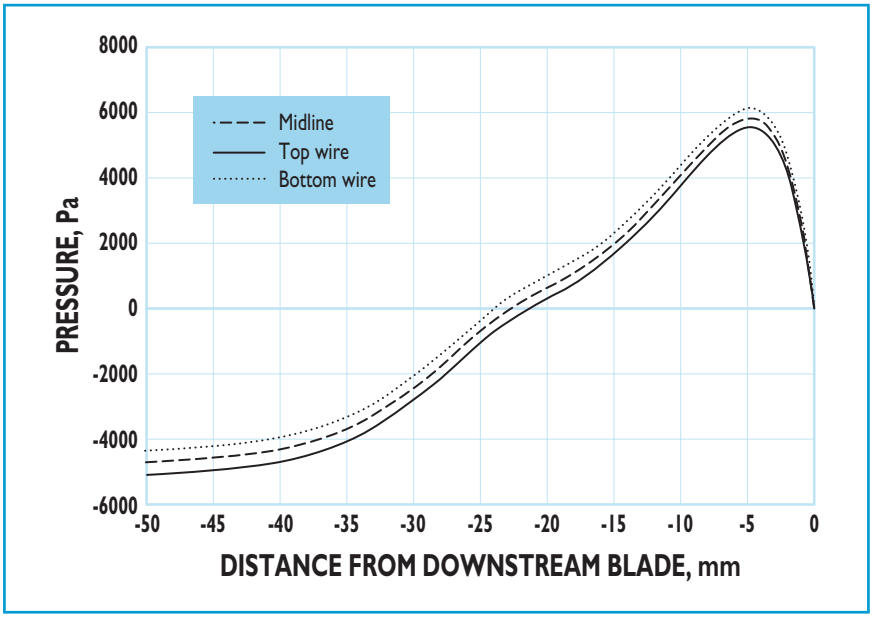

4. Pressure distribution between the forming fabrics, at three different locations in the gap, for the basic test case. The forming geometry is described in the text.

- The mass per unit area of the bottom wire with its adhering water layer and adhering fiber mat (M_1)
- The wire speed (V_o)
- The pressure underneath the bottom wire [$p_B(x)$]. Without a suction shoe present, this pressure is caused by the doctoring action of the blade on water adhering to the wire. With a suction shoe present, this pressure will be equal to the suction shoe pressure, p_s, plus the doctoring pressure.
- The bending stiffness of the top wire [$(EI)_2$]. The top wire does not come into physical contact with the blade.
- The tension per unit length in the top wire (T_2)
- The mass per unit area of the top wire with its adhering water layer and adhering fiber mat (M_2)
- The fluid density (ρ)
- The viscous shear stress exerted by the wire on the fluid between the wires (τ_w)
- A constant (C_2) that is a function of the headbox consistency, pulp furnish, and forming fabric.

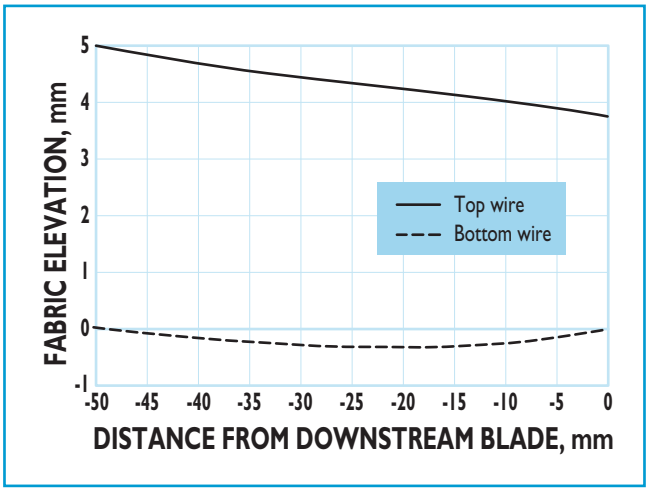

5. Top and bottom wire shapes for the forming geometry described in Fig. 4

Because the effect of wire bending stiffness is modest and computations including the bending stiffness are laborious *(3)*, the wire bending stiffnesses $(EI)_1$ and $(EI)_2$ were set to zero in the calculations that produced Figs. 4–8. The doctoring pressure, which has been considered previously, is set to zero here for simplicity. The viscous shear plays only a small roll in blade forming *(2)* and therefore is neglected.

In contrast with forming geometry simulations performed previously, modeling a suction shoe requires the solution of a two-point boundary value problem (the location of wire 1 is specified at both the first and the second blade). The two-point boundary value problem necessitates use of the shooting method in combination with the Runge-Kutta differential equation solver described earlier *(4)*.

RESULTS

A very large number of variables must be considered in the suction shoe twin-wire forming problem. All of the variables—such as the wire tensions, wire wrap angle, wire velocity, upstream wire gap size, etc.—considered in the study of single-blade forming are variables here, too. In addition, one must also allow for variable suction shoe pressure, variable separation distance between the blades, and variable starting drainage resistance on the two wires. To elucidate the effect of these different variables, different test cases, in which the variables mentioned previously are modified in turn, are presented in a future paper *(11)*. This paper will present the results of just a single test case.

Figure 4 shows the pressure pulse generated between two blades of a twin-wire former with the following characteristics:

- Wire velocity (V_o) = 16 m/s
- Backing wire tension (T_1) = 7000 N/m
- Conveying wire tension (T_2) = 7000 N/m

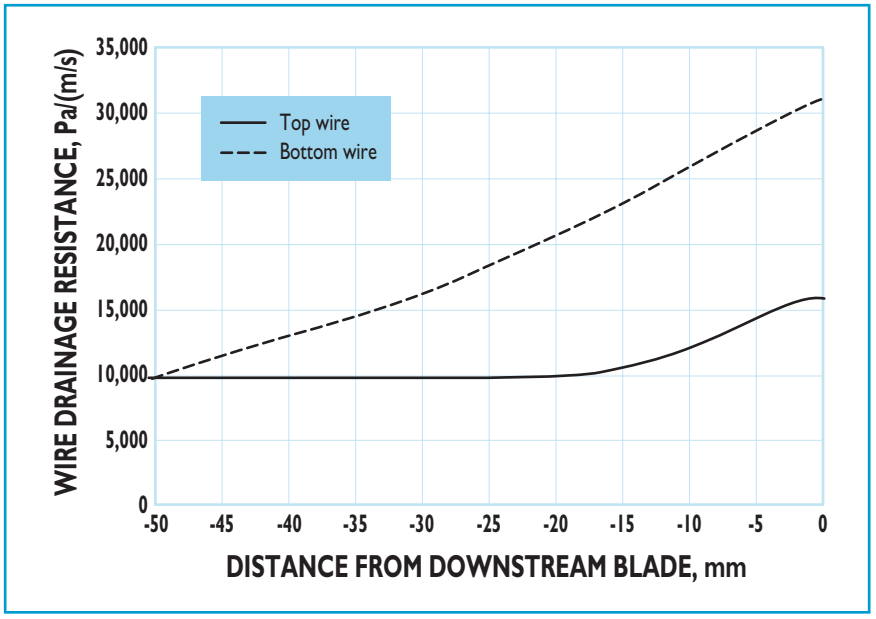

6. Drainage resistance of the top and bottom fabrics referred to in Fig. 4

- Wire wrap angle downstream of the downstream blade (α_2) = –0.03 radians
- Upstream gap size (H_o) = 5 mm
- Applied suction (p_s) = 7000 Pa
- Separation between blades (Δx) = 50 mm
- Bottom-wire upstream drainage resistance ($R_{1,o}$) = 10,000 Pa/(m/s)
- Top-wire upstream drainage resistance ($R_{2,o}$) = 10,000 Pa/(m/s)
- Drainage resistance variation constant (C_2) = 2×10^7 Pa/(m²/s)
- Mass per unit area of each fabric (M_1 and M_2) = 1.63 kg/m³.

Several features of Fig. 4 are quite interesting. Referring first to the midline pressure, note that near the blade, the pressure developed between the forming fabrics is similar to that produced by a blade without suction. Further from the blade, the pressure is strongly influenced by the suction shoe and takes a value about midway between the suction shoe pressure and atmospheric pressure. This intermediate pressure value is not unexpected. If the flow between the forming fabrics were purely rectilinear (i.e., the fabrics were without curvature) and the drainage resistances of the two fabrics were identical, according to Darcy's Law (and the Continuity Equation), the pressure between the fabrics would be precisely the average of the suction shoe pressure and the atmospheric pressure.

The curves labeled "top wire" and "bottom wire" in Fig. 4 refer to the pressures in the pulp suspension adjacent to the top wire and adjacent to the bottom wire, respectively. (Recall that the pressure difference between these locations is related to the curvature of the flow field, which causes centrifugal forces.) The pressure at the bottom wire is higher than the midline pressure, and the pressure at the top wire is less than the midline pressure, over the entire span between the blades. The values of these pressure differences are consistent with both the sign and magnitude of the centrifugal pressure effects discussed in relation to Eqs. 10 and 11.

One reviewer commented that the pressure profile shown in Fig. 4 is not periodic from one blade to the next. This non-periodicity is not an error in the program but is rather a result of two factors. As a result of fiber buildup on the forming fabrics as the fabrics pass downstream, there is no reason to believe that the pressure profiles will be periodic. Furthermore, for these simulations, I have specified that the fabric is straight downstream of the second blade. This implies that that blade is the last in the suction shoe and therefore would certainly not be expected to generate a pressure distribution similar to other blades in the shoe.

Figure 5 shows the shapes of the forming fabrics for this forming configuration. The bottom wire has the bowed shape that one would expect of a fabric sucked down between two fixed blades. The top wire, in contrast, has a nearly linear shape. The two shapes are very different owing to the effect of dewatering, which changes the gap between the fabrics.

The drainage resistance of the two fabrics, which is directly related to the thickness of the fiber mat accumulated on the fabrics, is plotted in **Fig. 6.** The resistance of the bottom wire increases continuously as the suction draws water out from between the fabrics, depositing the suspended fibers on the bottom-wire fabric. The pressure pulse generated by the downstream blade accelerates the fiber deposition. The application of suction also attempts to force water, from the exterior to the gap, through the top wire. This action is inhibited, however, by the action of the surface tension of the water–air interface in the small pores of the forming fabric, which is here posited to prevent the flow of water (and air) through the fabric[2]. When the pressure in the gap between the forming fabrics becomes positive, fiber deposition onto the top wire begins, resulting in its increased drainage resistance.

The local dewatering velocity through each fabric, plotted in **Fig. 7,** is simply the pressure difference

[2]If the applied suction were too great, air could be drawn between the fabrics. No attempt was made to model this complex two-phase flow phenomenon.

across the fabric divided by the local drainage resistance of the fabric (with its adhering fiber mat). For the top (non-blade-contacting) fabric, this pressure difference is equal to the pressure at the top wire (because gauge pressures are used). Since the gap pressure becomes positive within 22 mm of the blade, the drainage velocity becomes positive at the same location. Changes in the gap pressure are much greater than changes in the drainage resistance this close to the downstream blade, and therefore the dewatering velocity has a similar shape in this region to that of the pressure pulse. The bottom (blade-contacting) wire dewaters at a rate that is directly proportional to the difference between the bottom wire pressure and the applied suction and inversely proportional to its drainage resistance. The dewatering velocity first decreases, owing to the buildup of pulp fibers, which increases the fabric drainage resistance. Then, as the pressure pulse develops over the downstream blade, the drainage resistance variations occur slowly relative to the pressure changes; this causes the dewatering velocity to take a shape similar to that of the pressure pulse.

The pulp suspension flow between the forming fabrics is very nearly inviscid, and therefore the Bernoulli equation describes the flow well. According to this equation, the sum of the pressure in the gap and the dynamic pressure ($0.5\rho V_F^2$) is constant along the gap. A boundary condition for the flow at the downstream boundary is that the pressure is zero. This condition is required because the fabrics were assumed to be straight and parallel downstream of the blade. The fluid velocity is necessarily equal to the wire velocity because of the same constraint. The Bernoulli equation then indicates that wherever there is suction in the wire gap, the fluid velocity must exceed the wire velocity; the converse is true where the gap pressure is positive.

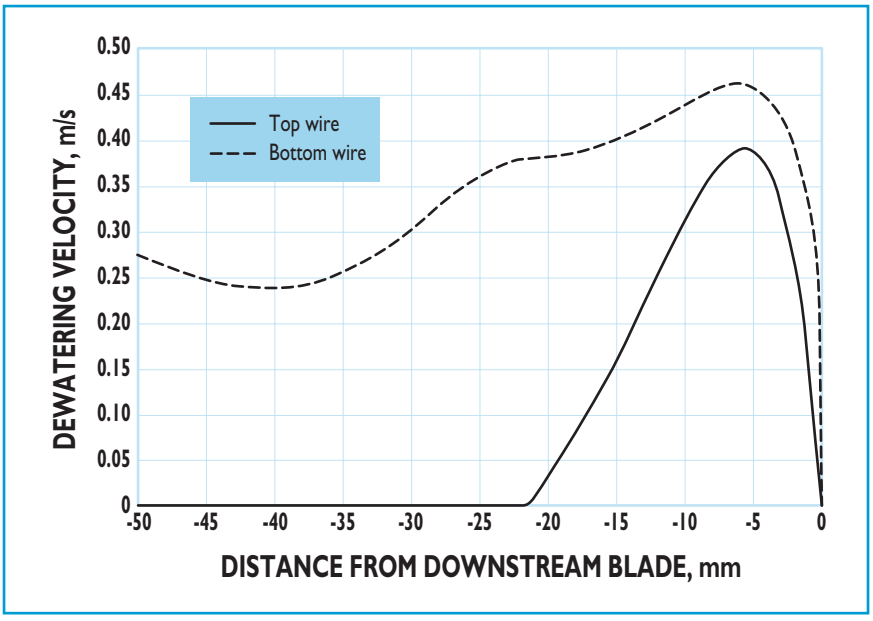

7. Dewatering velocity through the two forming fabrics for the geometry of Fig. 4

Figure 8 shows this behavior. Although explicable, the existence of local pulp velocities significantly different from the fabric velocity, far from the downstream blade, was somewhat disconcerting. In the follow-up paper, these local velocities are shown to be largely an artifact of the downstream pressure condition.

Consistency of results

No detailed measurements of pressures or dewatering rates in a paper machine with an operating suction shoe have been made. There have, however, been experimental measurements of fabric wrap angles around the blades in a suction shoe. These measurements will be compared with the computer simulation results in the companion paper. The simulation may also be readily compared with a global analysis of the suction shoe. That comparison is made as follows.

A vertical force balance on the top wire, from one blade in the suction shoe to the next, is written as follows:

$$\int p_2(x)dx = (T_2 - M_2 V_o^2)(\sin\alpha_{2,L} - \sin\alpha_{2,R}) \quad (17)$$

where $\alpha_{2,L}$ and $\alpha_{2,R}$ are, respectively, the angles made by the top fabric, relative to the horizontal, at the left blade and at the right blade. For the simulation described here, the wire angles were as follows:

$$\alpha_{2,L} = -0.03548 \text{ rad} \quad (17a)$$

$$\alpha_{2,R} = -0.030 \text{ rad} \quad (17b)$$

The theoretical integrated pressure for this configuration is as follows:

$$(7000 - 1.63\times16^2) \times [\sin(-0.03548) - \sin(-0.030)] = -36.01 \text{ Pa·m} \quad (17c)$$

For the simulation described previously, the actual integrated pressure was -37.17 Pa·m—only 3.2% different from the theoretical pressure.

A vertical force balance on the bottom wire, from one blade in the suction shoe to the next, may also be written:

$$-\int [p_1(x) - p_{SUCT}]dx = (T_1 - M_1 V_o^2)(\sin\alpha_{1,L} - \sin\alpha_{1,R}) \quad (18)$$

where $\alpha_{1,L}$ and $\alpha_{1,R}$ are, respectively, the angles made by the bottom fabric, relative to the horizontal, at the

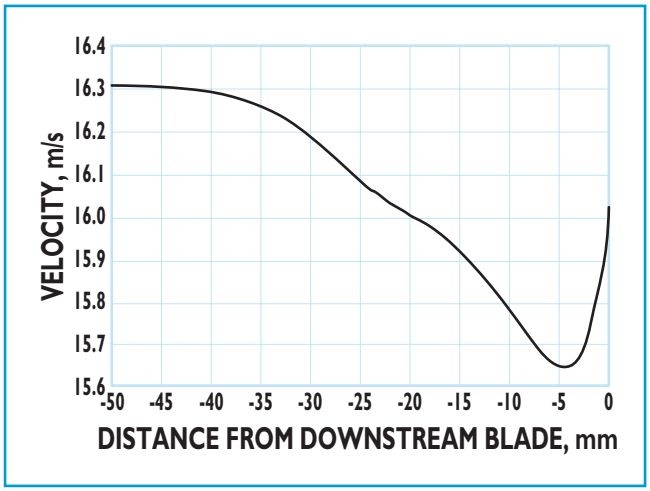

8. Pulp suspension velocity for the forming geometry described in Fig. 4

left blade and at the right blade. The wire angles were $\alpha_{1,L}$ = –0.03263 rad and $\alpha_{1,R}$ = 0.01928 rad. The theoretical integrated pressure for this configuration is as follows:

$$(7000 - 1.63\times16^2)\times[\sin(-0.03263) - \sin(0.01928)] = -341.6\ \text{Pa·m} \qquad (18a)$$

For the previously described simulation, the actual integrated pressure was –346.9 Pa·m—only 1.5% different from the theoretical pressure.

A second run of the simulation was done, except with the suction reduced to 3500 Pa. The simulated integrated pressure for wire 2 for this case was –42.5 Pa·m. This compares to a theoretical value, according to Eq. 17, of –43.4 Pa·m (a 2% error). Equation 18 predicts an integrated pressure of –231.2 Pa·m for wire 1. The simulated integrated pressure was –231.6 Pa·m (a 0.2% error).

The excellent agreement between the computer-simulation integrated pressures and the integrated pressures evaluated independently by means of a global force balance on each fabric suggests that the computer simulations are not unreasonable.

CONCLUSIONS

A computer simulation has been developed to model the behavior of a blade gap former with a suction shoe. The simulation includes the effects of variable mat drainage resistance on each of the forming fabrics and two-sided dewatering. The results of the simulation are plausible (i.e., consistent with our intuition) and are consistent with an independent global force balance to within a few percent. The detailed results of the simulation and a comparison with mill trials will be given in a future paper. **TJ**

Green is a professor at the University of British Columbia, Department of Mechanical Engineering, 2324 Main Mall, Vancouver V6T 1Z4, Canada.

The author gratefully acknowledges the support of his sponsors: Beloit Corp., JWI Ltd., MacMillan Bloedel, and NSERC. The author also appreciates the conversations he has had with Professor Richard Kerekes at UBC, Dr. Jay Shands at Beloit, and Graham Jackson, P.E. at JWI.

Received for review July 9, 1998.
Accepted Dec. 22, 1998.

LITERATURE CITED

1. Zhao, R. H. and Kerekes, R. J., *J. Pulp Paper Sci.* 21(3): J97(1995).
2. Green, S. I., *J. Pulp Paper Sci.* 23(7): J353(1997).
3. Green, S. I., Zhao, R. H., and Kerekes, R. J., *J. Pulp Paper Sci.* 24(2): J60(1998).
4. Green, S. I. and Kerekes, R. J., *TAPPI J.* 81(4): 180(1998).
5. Green, S. I., Roshanzamir, A., and Kerekes, R. J., *TAPPI 1997 Engineering Conference Proceedings,* TAPPI PRESS, Atlanta, p. 889.
6. Roshanzamir, A., Green, S. I., and Kerekes, R. J., *J. Pulp Paper Sci.* 24(11): 345(1998).
7. Zahrai, S. and Bark, F. H., *Nordic Pulp Paper Res. J.* 4: 245(1995).
8. Zahrai, S. and Bark, F. H., *AIChE Symp. Series* 92: 68(1996).
9. Zahrai, S., Bark, F. H., and Norman, B., *J. Pulp Paper Sci.* 23(9): J452 (1997).
10. Wildfong, V., Shands, J. A., Genco, M., *et al., TAPPI 1999 Engineering Conference Proceedings,* TAPPI PRESS, Atlanta, in press.
11. Green, S., *J. Pulp Paper Sci.,* in press.

OVERSIZED EQUATIONS

$$\frac{H}{(RC)} = \frac{(y_2 - y_1)}{2[1 + (dy_1/dx)^2]^2}\overline{d^2y/dx^2} + \frac{(y_2 - y_1)}{2[1 + (dy_2/dx)^2]^2}\overline{d^2y/dx^2} \qquad (12)$$

$$(EI)_1\frac{d^4y_1}{dx^4} - T_1\frac{d^2y_1}{dx^2} + M_1V_o^2\frac{d^2y_1}{dx^2} - p_B(x) + p_1 = 0 \qquad (13)$$

$$(EI)_2\frac{d^4y_2}{dx^4} - T_2\frac{d^2y_2}{dx^2} + M_2V_o^2\frac{d^2y_2}{dx^2} - p_2 = 0 \qquad (14)$$

$$V_F\left(\frac{dy_2}{dx} - \frac{dy_1}{dx}\right) + (y_2 - y_1)\frac{dV_F}{dx} + \frac{[p_1 - p_B(x)]}{R_1} + \frac{p_2}{R_2} = 0 \qquad (15)$$

$$\frac{dp}{dx} + \rho V_F\frac{dV_F}{dx} + \rho\left(\frac{[p_1 - p_B(x)]/R_1 + p_2/R_2}{(y_2 - y_1)}\right)[V_o - V_F] + \frac{2\tau_w}{(y_2 - y_1)} = 0 \qquad (16)$$